Available online at www.sciencedirect.com
ScienceDirect
Journal of the European Ceramic Society 30 (2010) 2009–2015
www.elsevier.com/locate/jeurceramsoc

Crystallization process of thermally treated vitrified EAFD waste

I. Tsilika, I. Eleftheriadis, Th. Kehagias *, E. Pavlidou, Th. Karakostas, Ph. Komninou

Physics Department, Aristotle University of Thessaloniki, GR-54124 Thessaloniki, Greece

Received 22 December 2009; received in revised form 24 March 2010; accepted 4 April 2010

Abstract

Electric arc furnace dust (EAFD) powder was mixed and vitrified with 55% SiO_2, 10% Na_2CO_3 and 35% $CaCO_3$ raw materials. The resulting glass was thermally treated at the same temperature at different annealing times. The process towards crystallization of the glass–ceramics produced, as a function of annealing time, was examined by means of optical microscopy, electron microscopy techniques and X-ray diffraction. While at small crystallization times wollastonite was the only crystalline phase separated from the amorphous matrix, as the time of crystallization increased crystals of diopside emanating from wollastonite were also observed. The emergence of diopside crystals was attributed to the tendency of the metallic elements of EAFD, incorporated in the wollastonite structure, to move towards the neighbouring glass matrix causing local maxima of concentration in the vicinity of wollastonite crystals. This diffusive motion of the metallic elements of EAFD, such as Fe, Zn, was found to follow the 2nd Fick law and plays a crucial role in the stability region of the crystallized structures of the system.

Keywords: Crystallization; Glass–ceramics; Electron microscopy; X-ray methods; Diffusion

1. Introduction

Pyroxenes and pyroxenoids are a polysomatic series of single chain silicates of the chemical formula $MSiO_3$ where M is Ca, Mg, Fe, Mn. The chains of the silica tetrahedra run parallel to the (1 0 0) direction and alternate with layers containing bands of divalent cations.[1] The periodicity of the silica tetrahedra and the arrangement of the divalent cations determine the various members of the series, being the end-member of the series pyroxenoid wollastonite and clinopyroxene. Wollastonite has a twisted chain with periodicity of 3, while clinopyroxene possesses a straight chain with periodicity of 2. Changes in pressure and temperature or cation size have been found to induce changes in the periodicity of the silica tetrahedra.[2]

Transformations from a clinopyroxene to a pyroxenoid (rhodonite, pyroxmagnite), by the increase of temperature or cation substitution have been reported in natural minerals.[3] The transformations observed by cation substitution depend on the relative amount and size of the substituted cation (Mg, Fe, Mn, Ca). Especially Ca, which is the largest cation, has been shown to cause substantial enlargement in the α and b cell dimensions.[4] Wollastonite (pyroxenoid) and diopside (pyroxene) are two crystalline phases that are frequently encountered in the glass–ceramics systems, containing industrial wastes, depending on the initial composition.[5–7] In a previous experiment,[8] the incorporation of EAFD waste in the SiO_2–CaO–Na_2O system to produce glass–ceramics, resulted in the formation of a pyroxenoid (wollastonite) as the only crystalline phase. Small divalent cations such as Mg, Fe, Mn, contained in EAFD, were found to be incorporated in the crystalline structure of wollastonite. The introduction of the foreign cations did not induce any transformation and caused only slight variations in the lattice parameters of wollastonite.

Pyroxenoid (bustamite) type of structure as the major crystalline phase was found also in cupola slag glass–ceramics by Agarwal et al.[9] At higher temperatures, bustamite turned into wollastonite (pyroxenoid) and diopside (pyroxene). As the holding time increased, diopside and wollastonite grew further at the expense of the initial bustamite type of structure.

In this contribution, we explore the crystallization process of thermally treated vitrified EAFD waste, where wollastonite and diopside crystal phases appear to separate from the matrix, by means of optical microscopy, X-ray diffraction and electron microscopy techniques, as a function of crystallization time. We elucidate the diffusive motion of the EAFD principal metallic elements (Fe and Zn) that activates the wollastonite to diop-

* Corresponding author. Tel.: +30 2310 998023; fax: +30 2310 998589.
E-mail address: kehagias@auth.gr (Th. Kehagias).

0955-2219/$ – see front matter © 2010 Elsevier Ltd. All rights reserved.
doi:10.1016/j.jeurceramsoc.2010.04.011

side transformation mechanism. The specific transformation, although not favoured by the composition of the vitrified system, is followed by drastic and abrupt changes in the amount and size of the substituted cations and therefore is not encountered in nature. This observation, along with the fact that glass–ceramics are systems with a route of formation and compositions different from natural rocks, turned the pyroxene–pyroxenoid phase transformation in synthesized glass–ceramics into the subject of our systematic investigation.

2. Experimental

Mechanically homogenised and refined EAFD powder, composition given in Refs. [10,11], was mixed with 55% SiO_2, 10% Na_2CO_3 and 35% $CaCO_3$ (wt%) powders. In particular, the composition chosen for the formation of vitreous products was the one found to demonstrate the best crystallization state (bulk crystallization), namely 15% EAFD, 55% SiO_2, 5% Na_2O, 25% CaO (wt%).[8] The mixture was placed in a Pt crucible and heated in an electric furnace at 1400 °C for 2 h, in ambient atmosphere. The melt was poured on a stainless steel plate and was rapidly cooled down at room temperature. The as-quenched vitreous product was then subjected to a two-stage isothermal treatment process at temperatures determined from differential thermal analysis (DTA) scans,[8,10] namely a nucleation stage at 680 °C for 15 min and then a crystal growth stage at 900 °C, for 15 min, 30 min, 2 h and 60 h.

The glass–ceramics products, E1, E2, E3 and E4, respectively, were structurally characterized by X-ray diffraction (XRD) analysis using a Seifert 3003 powder diffractometer and CuKa1 radiation. Scanning electron microscopy (SEM) observations and stoichiometric analysis of the materials were conducted in a JEOL JSM-840A microscope, equipped with an Oxford ISIS-300 energy dispersive X-ray spectrometry (EDXS) analyzer. Microstructural characterization was performed employing transmission electron microscopy (TEM) techniques. Samples for TEM were prepared by mechanical grinding followed by ion-milling to reach electron transparency. TEM observations were performed in a Jeol 2011 and a FEG scanning TEM (STEM) Jeol 2011 electron microscopes, both operated at 200 kV, the latter equipped with a Link EDXS microprobe analyzer capable of analyzing particles of a few nanometers size. The microprobe analysis was employed complementary to the EDXS analysis by SEM, where higher local resolution was demanded.

3. Results

3.1. Optical and scanning electron microscopy

The morphology of the crystals formed after annealing was studied by optical microscopy using transmitting light and SEM compositional images. It was observed that the formed crystals grew larger with increasing crystallization time, as expected. However, the variation of size as a function of crystallization time was not linear but increase of crystal sizes was more evident in the first two hours. As a result, after 60 h the size of the formed crystals was still relatively small compared to the prolonged crystallization time.

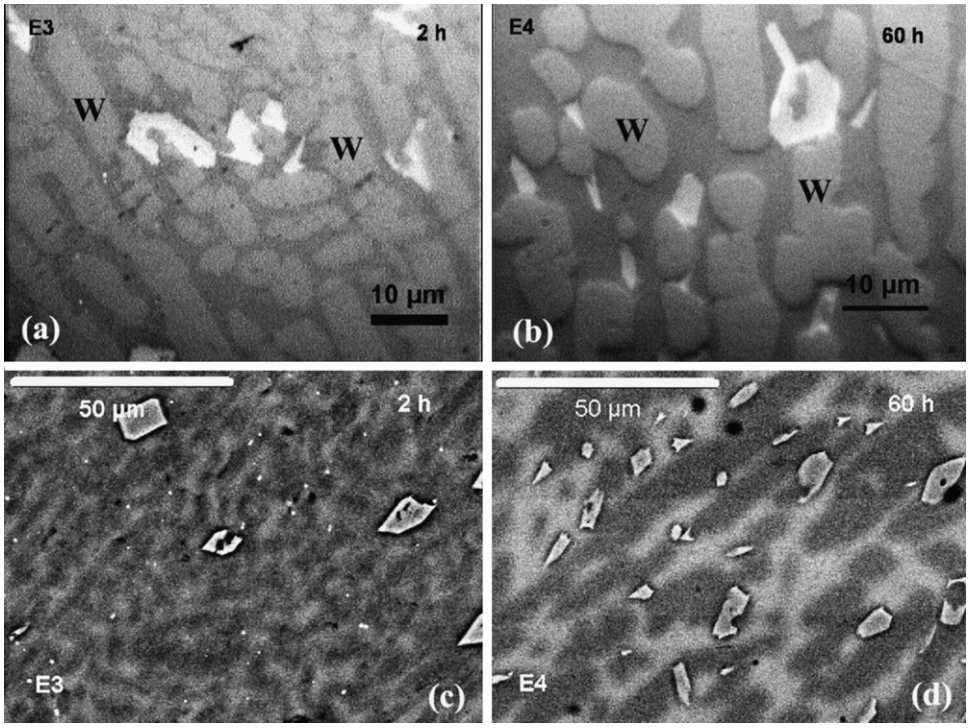

Fig. 1. (a) and (b) Optical micrographs of E3 and E4 glass–ceramics, showing the crystal phases (wollastonite (W) – bright contrast crystals, new phase – white crystals) separated from the vitreous matrix (darker contrast). (c) and (d) Corresponding SEM compositional images, showing the random distribution and sizes of the new phase crystals (white crystals), which are in contact with wollastonite.

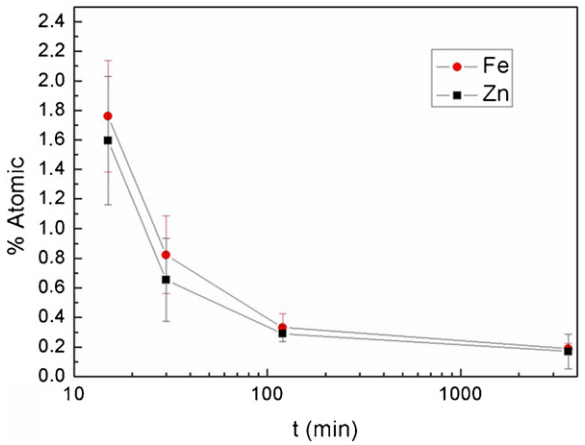

Fig. 2. Variation in the concentration of Fe and Zn EAFD elements in wollastonite crystals, as a function of crystallization time.

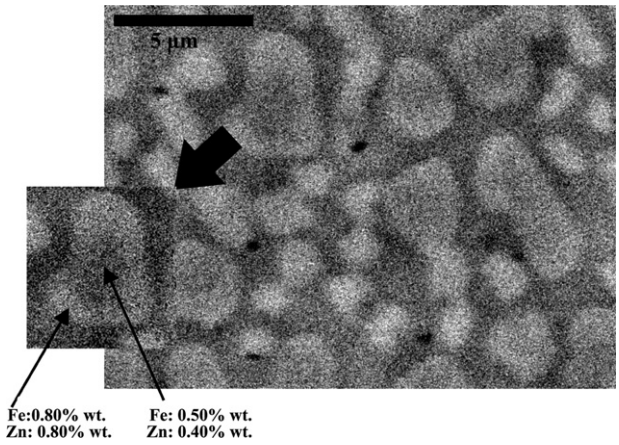

Fig. 3. SEM compositional image of E2 glass–ceramics, showing the change in the composition of Fe and Zn between the center and the edges of the wollastonite crystals.

In the glass–ceramics with 15 and 30 min crystallization times, wollastonite was the only crystal phase separated from the vitreous matrix, having a stoichiometry that revealed the incorporation of a significant amount of the metallic elements present in the EAFD.[8,10,11] Conversely, in the glass–ceramics with 2 and 60 h crystallization times, except wollastonite a new crystalline phase was observed to separate from the matrix (Fig. 1). Its crystals were observed to be systematically in contact with the wollastonite crystals, whereas their distribution seemed random and their size differed significantly from crystal to crystal. The main elements found in the new crystals from the EDXS analysis were Ca, Fe, Si, Zn, Mg Mn and O.

The distribution of the main metallic elements of EAFD, i.e. Fe and Zn, in the wollastonite crystals as a function of crystallization time was analyzed by EDXS in SEM. Hence, 10–15 measurements of each element's concentration at the center of the crystals of wollastonite in all the samples were taken. Their values along with the standard deviations are depicted in Fig. 2. The metallic elements were present, from the initial stages of crystal growth, within the crystal structure of wollastonite. As the time of crystallization increased, the presence of Fe and Zn in the crystal structure of wollastonite reduced almost exponentially. As a result, the initial 1.8–1.6 at% of Fe and Zn, respectively, after 15 min crystallization time, reduced to approximately 0.3 at% after almost 2 h. Further increase of the crystallization time, did not bring any significant changes in the composition of wollastonite. Simultaneously, an increase of the concentration of these elements in the adjacent to the crystals glass matrix was observed.

This diffusive motion of the EAFD elements from the crystals of wollastonite to the glass matrix maybe connected to the formation of the new phase, which seems to emerge integrating a part of these elements. The rest were gathered in the neighbouring to the crystals residual glass matrix and modified its composition. The tendency of the EAFD elements to move from the crystal structure of wollastonite to the vitreous matrix was also indicated in the SEM compositional images (Fig. 3). The crystallization time of 30 min seems to be enough to allow the movement of the metals, since the crystals of wollastonite showed a different contrast between the center and the edges, implying a different composition in the two regions. This difference can be attributed to the different concentration in elements of EAFD, which seems to be adequate to demonstrate the aforementioned tendency.

3.2. X-ray diffraction

The X-ray diffractograms of the E3 and E4 glass–ceramics are depicted in Fig. 4. E1 and E2 samples with crystallization time $t = 15$ and 30 min, respectively, exhibited wollastonite as the only phase crystallized, verifying previous observations.[8,10] Furthermore, in samples E3 and E4, the appearance a small peak at $\theta = 27.5^\circ$ and the broadening of the main reflection of wollastonite at $\theta = 30^\circ$ can be attributed to the emergence of the new crystal phase, which was observed by optical microscopy and SEM images. Taking the EDXS analysis into account, the new phase was identified as a diopside-like structure ($CaMgSi_2O_6$). An amorphous component evident in the diffractograms was due to the presence of the residual vitreous matrix.

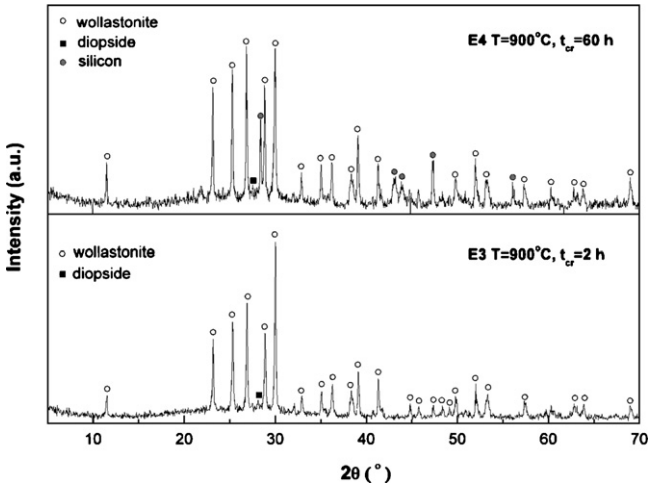

Fig. 4. X-ray diffractograms of E3 and E4 glass–ceramics showing the emergence of a diopside-like phase in the wollastonite dominated crystal structure of the glass–ceramics.

Table 1
Experimental values of θ (°) in wollastonite reflections.

Reflection	Triclinic wollastonite	E1, E2	E3	E4
2 0 0	23.158	23.178	23.175	23.156
0 0 2	25.302	25.340	25.330	25.307
−1 0 2	26.854	26.899	26.895	26.870
2 1 0	28.874	28.913	28.903	28.880
−2 2 0	29.972	30.033	30.018	29.987

In order to examine the influence of crystallization conditions on the lattice parameters of wollastonite, the exact positions of the X-ray reflections were determined. Therefore, 0.05 g of pure silicon was mixed with 0.5 g of each sample, as depicted in the X-ray diffraction pattern of the E4 sample (Fig. 4). The 1 1 1 reflection of Si was used as a reference for the correction of the angles of reflections from deviations that could be introduced by the diffractometer. The positions of the main experimental reflections were determined by fitting with Lorentzian curves and their values, together with the theoretical ones of triclinic wollastonite (Powder Diffraction File 84-6054), are shown in Table 1. The reflections of E1 and E2 were found at the same positions.

The measured values of E1, E2 and E3 reflections were shifted towards larger angles (namely smaller *d*-spacings) compared to the theoretical ones, which indicated ionic substitution of calcium by smaller cations, primarily Fe and Zn, and even Mn and Mg that exist in EAFD. The 0 0 2 and 2 0 0 reflections, which are directly related to the cell dimensions of wollastonite did not present any appreciable change as ionic substitution takes place in the [0 1 0] direction, along which the cations of calcium are arranged. As the time of crystallization increases from 15 min to 2 h, the positions of the reflections were shifted towards smaller angles (which correspond to larger *d*-spacings). After 60 h of annealing (E4 sample) the reflections were situated in almost the same positions as the theoretical ones, which reflected the depletion of wollastonite crystals from Fe and Zn atom species with increasing crystallization time.

3.3. Transmission electron microscopy

TEM was also employed, in order to examine thoroughly the microstructural changes brought in the crystallization state, as the time of crystallization increases. In samples E1 and E2 with the smaller crystallization time, 15 and 30 min, respectively, selected area electron diffraction (SAED) patterns showed wollastonite (triclinic and monoclinic) as the only crystalline phase (Fig. 5(a) and (b)). Due to the close structural and energy relation of the two polytypes of wollastonite, the reflections of monoclinic and triclinic wollastonite could not be distinguished in the x-ray diagrams. Faulted structures of triclinic wollastonite, i.e. structures with the lattice angles (α, β, γ) of triclinic wollastonite and the lattice parameters (a, b, c) of monoclinic wollastonite were also observed (Fig. 5(c)). In the particular structures, the nanoprobe EDXS analysis showed that the elements of EAFD participate in the crystal structure of wollastonite (Table 2). In the SAED patterns derived from faulted crystals with a high

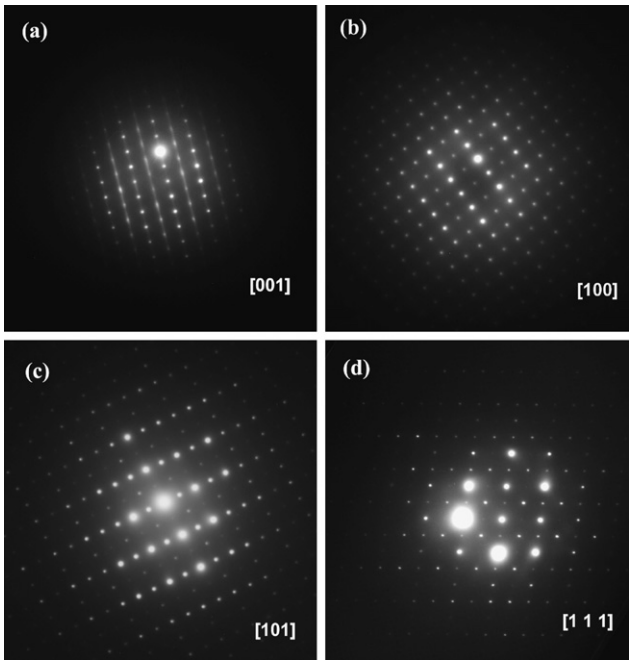

Fig. 5. SAED patterns of wollastonite crystals: (a) triclinic, sample E2, zone axis [0 0 1]; (b) monoclinic, sample E2, zone axis [1 0 0]; (c) faulted triclinic wollastonite, sample E2, zone axis [1 0 1]; (d) monoclinic wollastonite with superlattice reflections, sample E1, zone axis [1 1 1].

percentage of EAFD elements, a superlattice seems to be created (Fig. 5(d)). In larger crystallization times (2 h – sample E3), small rectangular or orthogonal crystals appear at the edges of wollastonite crystals, as depicted in the TEM image of Fig. 6, and can be directly attributed to the new phase, identified as diopside-like from XRD analysis.

In order to undoubtedly characterize the new separated crystal phase in high crystallization times, a number of high symmetry SAED patterns were obtained from various single crystallites. Wide-angle tilt-rotation TEM experiments were carried out to determine the characteristic extinction rules of the different reflections. The experimental procedure comprises the detection of at least one high symmetry zone axis of the new crystal phase, followed by successive tilting about a low indices reflection belonging to the initial zone and rotating, repeatedly about another low indices reflection when a new high symmetry zone axis is placed parallel to the electron beam. The corresponding SAED patterns that are illustrated in Fig. 7 were formed from the superposition of two structures. The high intensity reflections were identified as the clinopyroxene (diopside) type of structure, whereas the weaker intensity reflections were attributed to monoclinic wollastonite. Faulted structures of wollastonite

Table 2
Microprobe EDXS analyses of wollastonite crystals composition (at%) corresponding to the SAED patterns of Fig. 5(a)–(c).

	Si	Ca	Fe	Zn	Mn	O
SAED 5(a)	25.40	20.20	0.10	0.10	0.00	54.20
SAED 5(b)	20.20	17.60	0.20	0.20	0.15	61.80
SAED 5(c)	23.25	13.30	1.20	0.80	0.20	61.30

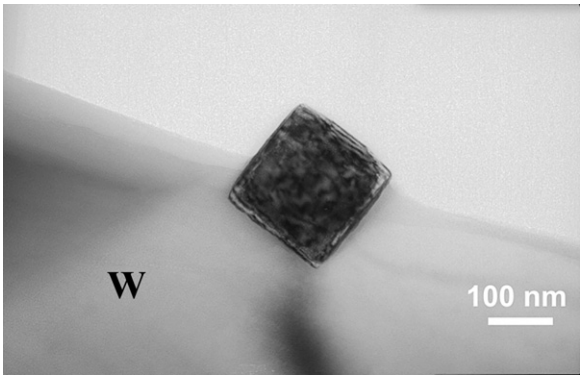

Fig. 6. Bright field (BF) TEM images of a crystal of wollastonite (W) in E3 glass–ceramic, where a new crystal phase of rectangular geometry is evident. The new crystals are formed at the edges of wollastonite crystals.

(monoclinic or triclinic) were not detected in this sample. This diopside type of structure possesses lattice parameters close to that of wollastonite but with deviations in the stoichiometry compared to the ideal structure. Nevertheless, the new phase can be characterized as diopside.

Crystallization times of 60 h led to the formation of independent crystals of diopside and wollastonite. The crystals of diopside have the characteristic polygonal shapes and white colour that was observed in the SEM images. The EDXS microprobe analysis showed the existence of Ca, Si, Fe, Zn, Mg and Na in their structure, as shown in Fig. 8. The crystals of wollastonite (triclinic and monoclinic) do not seem to contain elements of EAFD in their structure. It is worth notic-

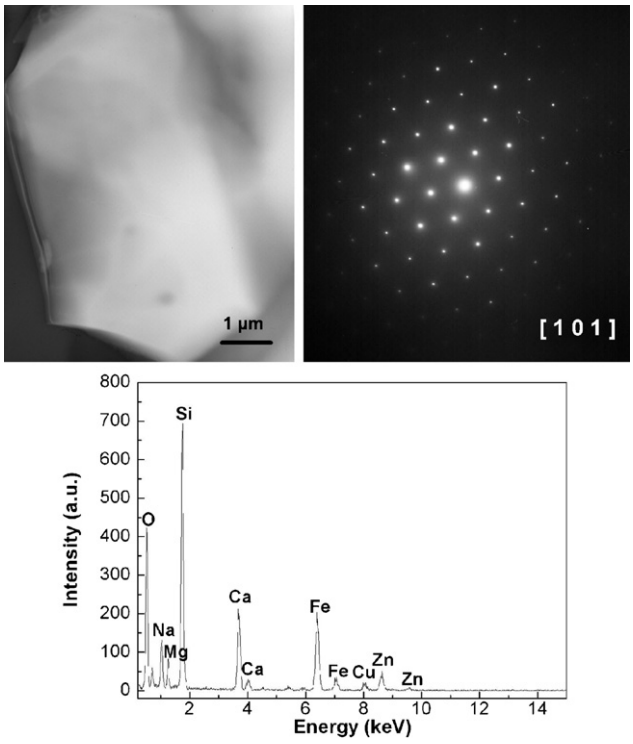

Fig. 8. (a) BF image of a diopside crystal in E4 glass–ceramics; (b) and (c) the corresponding SAED pattern and microprobe EDXS analysis.

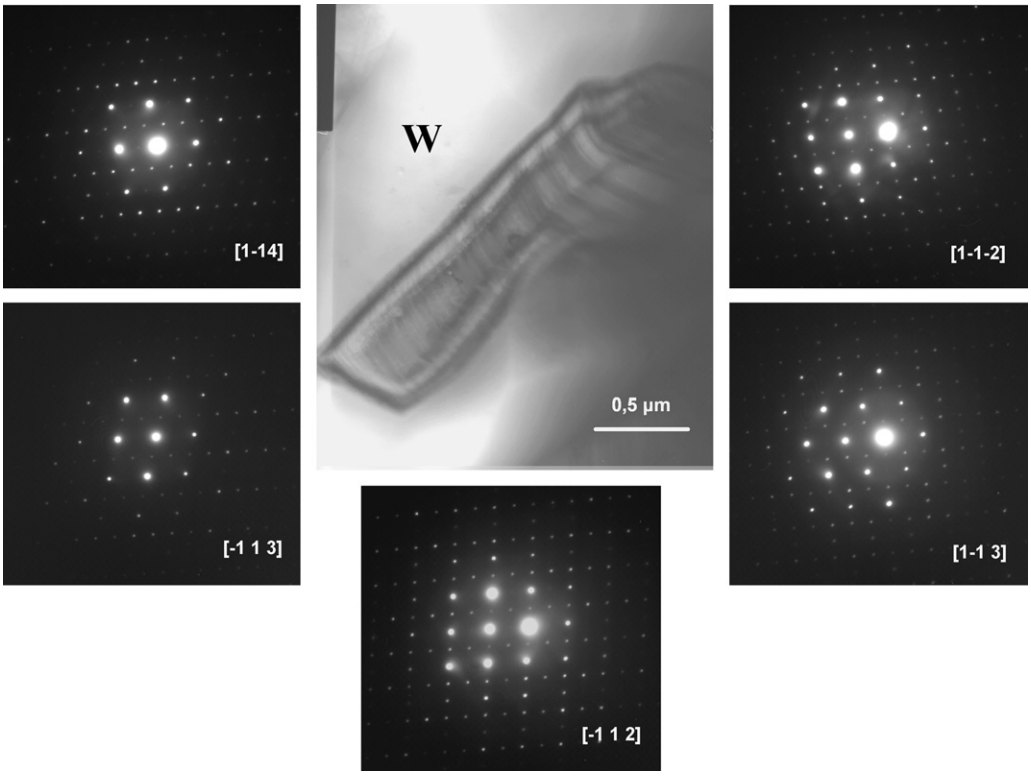

Fig. 7. BF TEM image of a rectangular geometry crystal of a clinopyroxene on top of a wollastonite crystal in E3 glass–ceramics. The zone axis, in each SAED pattern, corresponds to a clinopyroxene (diopside) type of structure.

ing that magnesium appeared only in the crystals of diopside and was absent from wollastonite. This behaviour of magnesium is well known from studies in the natural minerals of wollastonite.[12]

4. Discussion

In the present experiment the composition of the samples favoured the creation of the pyroxenoid wollastonite as the main crystalline phase, as it was found from XRD and TEM measurements. The cations of Fe, Zn, Mg, Mn, contained in EAFD, even though they are smaller compared to Ca, were not adequate to induce phase transformations and the formation of the lower energy pyroxene structures. As a result, they were arranged in the larger octahedral sites of Ca in the wollastonite structure, causing the shrinkage of the lattice constants in wollastonite and as consequence the observed shift in the position of the reflections in the diffractograms and in the measured values of the *d*-spacings of the SAED patterns.

At smaller crystallization times (15 and 30 min) the presence of the Fe, Zn, Mn cations in the structure was more intense, causing the formation of distorted structures of wollastonite (monoclinic and triclinic) and local stresses. As the time of crystallization increases, the reflections tend to approach the values of the undistorted wollastonite. At 60 h crystallization time, the EAFD elements were almost absent from the structure of wollastonite, which means that the phenomenon of ionic substitution that was dominant in the first half an hour, became unimportant with increasing time. This was consistent with EDXS measurements in the crystals of wollastonite, which showed that the concentration of EAFD elements in the crystal structure was substantial in the beginning of crystal phase separation and was reduced almost exponentially with the increase of the crystallization time.

In fact, the experimentally observed progressive movement of Fe and, Zn species, from the wollastonite crystals towards their edges seems to obey the 2nd Fick law of diffusion, which is applicable in monocrystals. The 2nd Fick law in one dimension takes the form[13] of Eq. (1), where c is the concentration of the species and D is the diffusion coefficient. For a steady concentration of a material that surrounds a host material in the form of a very thin layer and is subjected to thermal treatment at a temperature T and time t, the solution of Eq. (1), taking into account the boundary conditions $c(x = \pm\infty \rightarrow 0)$ and the initial condition $c(x,0) = M\delta(x)$ takes the form[13] of Eq. (2), where M is the initial mass of the elements that are introduced inside the host material. For $x = 0$ (the source of the material) Eq. (2) transforms into Eq. (3). By taking the logarithms in both sides of Eq. (3) we end up in a linear relation between $\log c$ and $\log t$, Eq. (4), where the constant α relates the initial mass of the material (element) with the diffusion coefficient and can be denoted as the *constant parameter in the diffusion equation* (Eq. (5)).

$$\frac{\partial c}{\partial t} = D\frac{\partial^2 c}{\partial x^2} \tag{1}$$

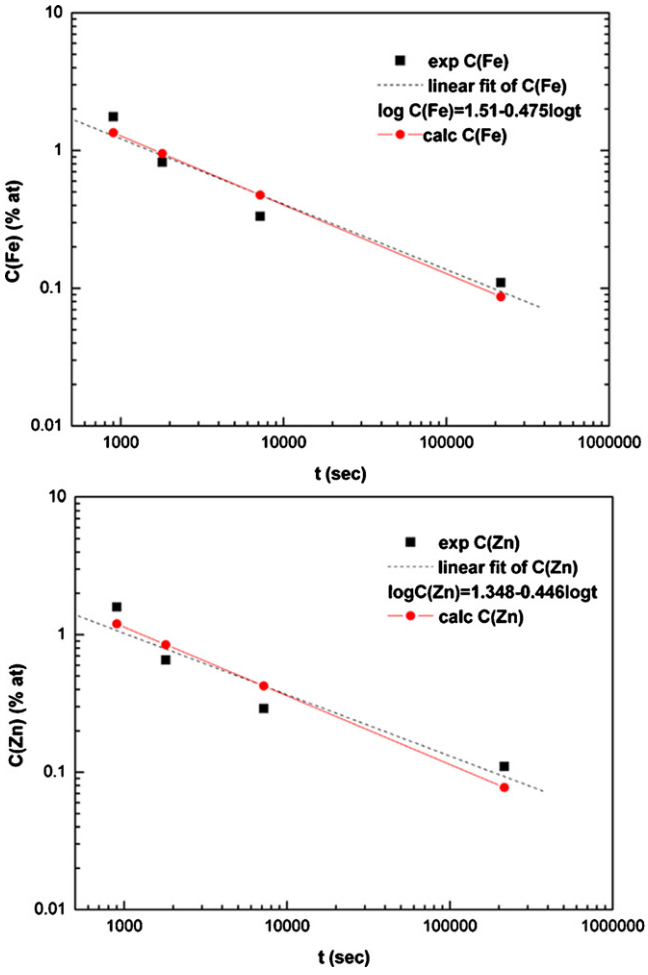

Fig. 9. Experimental and calculated values of the concentration of Fe, Zn elements as a function of crystallization time.

$$c(x,t) = \frac{M}{2\sqrt{\pi Dt}}\ \exp\left(-\frac{x^2}{4Dt}\right) \tag{2}$$

$$c(0,t) = \frac{M}{2\sqrt{\pi Dt}} \tag{3}$$

$$\log c = \log\alpha - \frac{1}{2}\ \log t \tag{4}$$

$$\alpha = \frac{M}{2\sqrt{\pi D}} \tag{5}$$

In our experiment, we assume that $x = 0$ (the source of the elements) is the center of the wollastonite crystals. As it is apparent from Fig. 9(a) the theoretical values of concentration of Fe (calc C(Fe)), calculated by Eq. (4), are very close to the experimentally measured ones (exp C(Fe)), which means that the tendency of the Fe, Zn elements to move from the wollastonite crystals towards their edges obey the 2nd Fick law of diffusion. Furthermore, the slope of the fitted to the experimental values line was found to be −0.475 a value close to −0.5 of Eq. (4) (Fig. 9a). The same applies also to Zn, but in this case the slope of the fitted line was found equal to −0.445, which is smaller than the expected −0.5 (Fig. 9(b)). The constant parameters in the diffusion equation where found $\alpha_{Fe} = 32.36$ and $\alpha_{Zn} = 22.28$.

The observed diffusion of Fe, Zn elements in the crystals of wollastonite towards the neighbouring vitreous matrix led to the formation of diopside as second crystalline phase, that of diopside, at crystallization times of 2 and 60 h, which was observed in optical microscopy and SEM and was positively identified by XRD and TEM. This crystalline phase belongs to the pyroxene family and grows in contact with wollastonite. The crystallization of diopside was fast and completed in short times.[14] This explains why the size of the crystals does not exhibit any observable change in the time interval of 2–60 h. The crystals of diopside do not appear from the beginning of crystallization during the nucleation process and thus, their crystallization is not observed in the DTA thermographs. According to previous observations,[8] the elements of EAFD in the glass–ceramics act as nucleating agents, which favour the formation of wollastonite. During the crystallization process, the EAFD elements are diffused in the neighbouring glass matrix. At short crystallization times, it would be expected the elements of EAFD to be found inside the structure of wollastonite in the calcium sites that was indeed observed. As the time of crystallization increases, the lattice relaxed through the diffusion of the cations of Fe, Zn in the nearby glass matrix. During the diffusion process, the cations were gathered in the surroundings of wollastonite crystals causing local maxima of concentration. The presence of these elements in large concentrations at the borders of wollastonite crystals favoured the transformation of the pyroxenoid wollastonite to the pyroxene diopside. In our case, the particular transformation that is in practice an order–disorder transformation starts at 30 min with the formation of short-range order structures, which evolved in the separated crystal phase of diopside at prolonged annealing times.

The increase in the crystallization time led also to the increase of the crystal size without affecting the percentage of crystallization, as it was made apparent by the X-ray diagrams.

5. Conclusions

To sum up, the crystallization of EAFD waste vitrified with SiO_2, Na_2O, CaO raw materials at small crystallization times (15 and 30 min) resulted in the production of glass–ceramics with wollastonite as the only crystalline phase. As the crystallization time increases, a second phase of diopside separated from the matrix, although the composition of the system does not favour its formation. The crystals of diopside were found in close contact with wollastonite crystals and their formation is explained through the mechanism of cationic substitution. This transformation was attributed to the tendency of the EAFD elements to diffuse with time from the center to the edges of the wollastonite crystals and to the neighbouring glass matrix. The diffusion was proved to follow the 2nd Fick law of diffusion applied in monocrystals. Due to the nature of the diffusion mechanism that drove the pyroxenoid (wollastonite) to diopside (clinopyroxene) transformation, the crystallization time had played a crucial role in the stability region of the two structures. The comprehension of the mechanism of crystallization of diopside allows us to determine the appropriate conditions that favour the formation of certain structures.

Acknowledgements

This work was co-funded by the European Social Fund and National resources, through the "PYTHAGORAS II" program.

References

1. Prewitt CT, Peacor PR. Crystal structure of the pyroxenes and pyroxenoids. *Am Miner* 1964;**49**:1527–42.
2. Pinckney LR, Burnham CW. Effects of compositional variation on the crystal structures of pyroxmangite and rhodonite. *Am Miner* 1988;**73**:798–808.
3. Veblen PR. TEM study of pyroxene-to-pyroxenoid reaction. *Am Miner* 1985;**70**:885–901.
4. Pinckney LR, Burnham CW. High-temperature crystal structure of pyroxmangite. *Am Miner* 1988;**73**:809–17.
5. Alizadeh P, Marghussian VK. Study of bulk crystallization in $MgO–CaO–SiO_2–Na_2O$ glasses in the presence of CaF_2 and MoO_3 nucleant. *J Mater Sci* 2003;**38**:1529–34.
6. Alizadeh P, Marghussian VK. The effect of compositional changes on the crystallization behavior and mechanical properties of diopside-wollastonite glass ceramics in the $SiO_2–CaO–MgO$ (Na_2O) system. *J Eur Ceram Soc* 2000;**20**:765–73.
7. Romero M, Rincon JMa, Rawlings RD, Boccaccini AR. Use of vitrified urban incinerator waste as raw material for production of sintered glass ceramics. *Mater Res Bull* 2001;**36**:383–95.
8. Tsilika I, Komninou Ph. Structural characterization of $Na_2O–CaO–SiO_2$ glass ceramics reinforced with Electric Arc Furnace Dust. *J Eur Ceram Soc* 2007;**27**:2423–31.
9. Agarwal G, Hong KS, Fletcher MR, Speyer RF. Crystallization behavior of cupola slag glass ceramics. *J Non-Cryst Solids* 1991;**130**:187–97.
10. Kavouras P, Ioannidis ThA, Kehagias Th, Tsilika I, Chrissafis K, Kokkou S, et al. EAFD-loaded vitreous and glass–ceramic materials. *J Eur Ceram Soc* 2007;**27**:2317–23.
11. Kavouras P, Kehagias Th, Tsilika I, Kaimakamis G, Chrissafis K, Kokkou S, et al. Glass-ceramic materials from electric arc furnace dust. *J Hazard Mater* 2007;**139**:424–9.
12. Mason B. Compositional limits of wollastonite. *Am Miner* 1975;**60**:209–12.
13. Shewmon PG. *Diffusion in solids*. New York: M Graw Hill; 1963, pp 1–47.
14. Abdel-Hameed SAM. Development of wall covering glass ceramics from raw materials. *Glass Sci Technol* 2002;**75**:290–3.